Inorg. Chem. **2006**, *45*, 4346−4351

The Room-Temperature Superstructure of ZrP_2O_7 Is Orthorhombic: There Are No Unusual 180° P–O–P Bond Angles

Henrik Birkedal,*[,†,#] Anne Marie Krogh Andersen,[‡] Alla Arakcheeva,[†,§] Gervais Chapuis,[†] Poul Norby,[||] and Philip Pattison[†,⊥]

Laboratory of Crystallography, Ecole Polytechnique Fédérale de Lausanne, BSP Dorigny, CH-1015 Lausanne, Switzerland, Department of Structural Chemistry, Arrhenius Laboratory, Stockholm University, S-10691 Stockholm, Sweden, Baykov Institute of Metallurgy and Materials RAS, Leninskii pr. 49, 119991 Moscow, Russia, Department of Chemistry, University of Oslo, P.O. Box 1033, Blindern, N-0315 Oslo, Norway, and Swiss−Norwegian Beam Lines, European Synchrotron Radiation Facility, BP-220, F-38043 Grenoble Cedex, France

Received January 5, 2006

The structure of room-temperature ZrP_2O_7 is shown to be orthorhombic by a combination of high-resolution synchrotron powder diffraction and single-crystal synchrotron diffraction data. Small nontwinned single crystals were obtained by synthesizing the compound using solvothermal methods at temperatures below the cubic to orthorhombic phase transition. The average P–O–P angle is 146°. DFT calculations (B3LYP/AUG-cc-pVDZ) on the isolated $P_2O_7^{4-}$ anion yield a P–O–P angle of 153.42° and indicate that the barrier to inversion is of the order 3.6 kJ mol^{-1}.

Introduction

The pyrophosphate compounds, MA_2O_7 (M = Si, Ge, Sn, Pb, Ti, Zr, Hf, U, Th, etc.; A = V, P), have recently attracted great interest because of the presence of phases with very low or even negative thermal expansion.[1−3] Of the compounds studied so far, ZrV_2O_7 and HfV_2O_7 demonstrate negative thermal expansion.[4] This difference in behavior appears to influence also the response of the compounds to high pressure: ZrP_2O_7 and TiP_2O_7 contract smoothly up to at least 20.5 and 40.3 GPa, respectively. ZrV_2O_7, on the other hand, undergoes a cubic to orthorhombic phase transition around 1.38−1.58 GPa and becomes X-ray amorphous above 4 GPa.[5] Common to the entire family is the presence of a high-temperature low-volume cubic ($Pa\bar{3}$) structure. This phase undergoes a phase transition to a low-temperature (LT) $3 \times 3 \times 3$ superstructure, that is, with a 27-fold increase in unit cell volume. Only a few of these compounds have been structurally characterized in the LT phase, and they are all cubic ($Pa\bar{3}$). This is the case for ZrV_2O_7,[6] TiP_2O_7,[7] and SiP_2O_7.[8] However, it has been shown by laboratory powder X-ray diffraction that the superstructure phase of GeP_2O_7 is at least monoclinic ($P2_1/c$) or possibly even triclinic.[9] MoP_2O_7 has been reported to have a cubic metric but orthorhombic symmetry by single-crystal diffraction, but the data did not allow satisfactory structure determination.[10] SnP_2O_7 has been shown by advanced solid-state NMR techniques to be monoclinic, space group $P2_1$ or Pc.[11]

The LT to high-temperature (HT) phase transition has been reported to occur at 290 °C in ZrP_2O_7.[12] Recently the

* To whom correspondence should be addressed. E-mail: hbirkedal@chem.au.dk. Phone: +45 8942 3887. Fax: +45 8619 6199.
† Ecole Polytechnique Fédérale de Lausanne.
# Present address: Department of Chemistry and Interdisciplinary Nanoscience Center, University of Aarhus, Langelandsgade 140, DK-8000 Aarhus C, Denmark.
‡ Stockholm University.
§ Baykov Institute of Metallurgy and Materials RAS.
|| University of Oslo.
⊥ European Synchrotron Radiation Facility.

(1) Sleight, A. W. Compounds That Contract on Heating. *Inorg. Chem.* **1998**, *37*, 2854−2860.
(2) Sleight, A. W. *Annu. Rev. Mater. Sci.* **1998**, *28*, 29−43.
(3) Evans, J. S. O. *J. Chem. Soc., Dalton Trans.* **1999**, 3317−3326.
(4) Khosrovani, N.; Sleight, A. W.; Vogt, T. *J. Solid State Chem.* **1997**, *132*, 355−360.
(5) Carlson, S.; Krogh Andersen, A. M. High-Pressure Properties of TiP_2O_7, ZrP_2O_7 and ZrV_2O_7. *J. Appl. Crystallogr.* **2001**, *34*, 7−12.
(6) Evans, J. S. O.; Hanson, J. C.; Sleight, A. W. *Acta Crystallogr., Sect. B* **1998**, *54*, 705−713.
(7) Norberg, S. T.; Svensson, G.; Albertsson, J. *Acta Crystallogr., Sect. C* **2001**, *57*, 225−227.
(8) Tillmanns, E.; Gebert, W.; Baur, W. H. *J. Solid State Chem.* **1973**, *7*, 69−84.
(9) Losilla, E. R.; Cabeza, A.; Bruque, S.; Aranda, M. A. G.; Sanz, J.; Iglesias, J. E.; Alonso, J. A. *J. Solid State Chem.* **2001**, *156*, 213−219.
(10) Haushalter, R. C.; Mundi, L. A. *Chem. Mater.* **1992**, *4*, 31−48.
(11) Fayon, F.; King, I. J.; Harris, R. K.; Gover, R. K. B.; Evans, J. S. O.; Massiot, D. Characterization of the Room-Temperature Structure of SnP_2O_7 by ^{31}P Through-Space and Through-Bond NMR Correlation Spectroscopy. *Chem. Mater.* **2003**, *15*, 2234−2239.

10.1021/ic0600174 CCC: $33.50
Published on Web 04/26/2006

observation of an intermediate incommensurate phase has been reported in a narrow temperature range around the phase transition.[13] The structure of the LT phase of ZrP_2O_7 was discussed by Khosrovani et al. on the basis of neutron powder diffraction data.[14] Their analysis assumed space group $Pa\bar{3}$, which restricts some of the P−O−P bond angles to 180° on average and contains 11 independent P sites. However, solid-state ^{31}P NMR data would suggest that there are more than 11 P sites. In the original report on the $ZrV_{2-x}P_xO_7$ series, this disaccord was assumed to be due to an impurity.[12] Very recently, however, advanced 2D solid-state ^{31}P NMR techniques, like those used for SnP_2O_7,[11] were used to unequivocally show that all the observed peaks in the ^{31}P NMR MAS spectra originate from the same phase and that there are 27 distinct ^{31}P resonances corresponding to 13 $P_2O_7^{4-}$ units with two inequivalent P sites and one $P_2O_7^{4-}$ unit with two equivalent P sites. These observations point to the space group *Pbca*.[15]

To shed light on these disparities in the literature, we decided to study the room-temperature structure of the LT phase of ZrP_2O_7 using high-resolution crystallographic techniques. As we will show in this paper, the combination of very high-resolution synchrotron powder diffraction and area detector synchrotron single-crystal diffraction is exactly what is needed to tackle this type of complex problem (a combination of very small lattice distortions, only small single crystals available, and many weak superstructure reflections). These methods have allowed us to determine unequivocally that the LT phase of ZrP_2O_7 is orthorhombic and does not reveal any 180° P−O−P bond angles.

Experimental Section

Synthesis. Single crystals of ZrP_2O_7 were prepared by solvothermal treatment of amorphous zirconium phosphate with phosphoric acid. In the preparations, 1.5 g of amorphous zirconium phosphate prepared as in ref 16 and 10 mL of 89% H_3PO_4 were mixed in a Teflon-lined autoclave. The resulting gel was slowly heated to 240 °C and kept at this temperature for 48 h. After cooling, the crystals were separated from the liquid by centrifugation, washed with water, and air-dried.

The chemical composition was verified using an ARL−SEMQ microprobe. Scans for other elements were negative. Elemental analysis (Zr, P) was performed on several crystallites using baddelyte (ZrO_2) and apatite ($Ca_5(PO_4)_3OH$) as reference materials. No deviation from nominal composition was detected (with an average of 8 measurements out of 10 with 2 outliers rejected, a composition of $ZrP_{2.14(5)}O_{6.88(10)}$ was obtained). A scanning electron microscopy picture taken on a Cambridge Stereoscan 150 of the crystals is shown in Figure 1 and illustrates the pseudocubic morphology of the crystals.

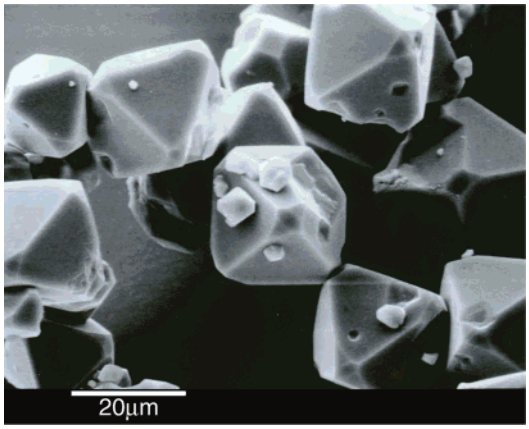

Figure 1. SEM image of the ZrP_2O_7 crystals at 1400× magnification.

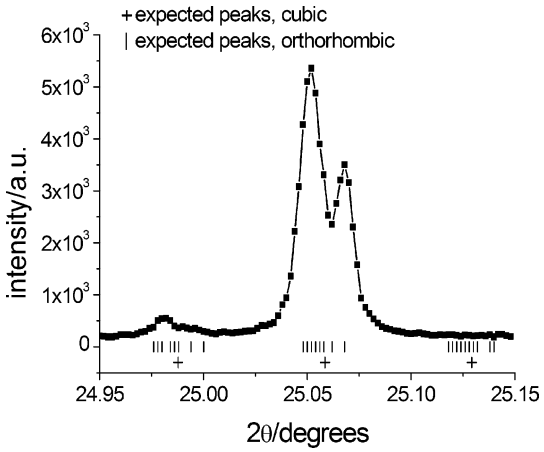

Figure 2. High-resolution synchrotron powder diffraction data of ZrP_2O_7 collected at room temperature. Expected peak positions are shown as plus signs and vertical lines for cubic and orthorhombic symmetry, respectively. The strong peak at 25.06° is (0 6 12) in the cubic indexation. Note the clear peak splitting, which proves that the symmetry is lower than cubic.

High-Resolution Synchrotron Powder Diffraction. Room-temperature synchrotron high-resolution powder diffraction (HRPD) data were measured at the station BM01B of the Swiss−Norwegian Beam Lines (SNBL) at the European Synchrotron Radiation Facility (ESRF), Grenoble, France. The wavelength, selected by a parallel geometry Si(111) channel-cut monochromator and refined with a Si standard, was $\lambda = 0.8000$ Å. The sample was loaded in a glass capillary, and the diffracted beam was analyzed with a Si(111) analyzer to increase angular resolution. The resulting data, covering $2\theta = 20.018-31.998°$ with a step size of 0.002°, clearly showed deviations from cubic symmetry (see Figure 2). The data set was used for refinement in general structure analysis system (GSAS).[17] The intensities were obtained from the single-crystal model (see below) in order to ensure a correct distribution of intensity between the closely spaced peaks. The fit converged at $R_{wp} = 0.0836$, $R_p = 0.0699$, and $\chi^2_{reduced} = 1.489$ for 12 profile parameters (*a*, *b*, *c*, zero-point, GW, LY, and six background coefficients) and at $R(F^2) = 0.0913$ for 2025 observations. The resulting lattice constants are given in Table 1.

(12) Korthuis, V.; Khosrovani, N.; Sleight, A. W.; Roberts, N.; Dupree, R.; Warren, J. W. W. Negative Thermal Expansion and Phase Transitions in the $ZrV_{2-x}P_xO7$ Series. *Chem. Mater.* **1995**, *7*, 412−417.

(13) Withers, R. L.; Tabira, Y.; Evans, J. S. O.; King, I. J.; Sleight, A. W. *J. Solid State Chem.* **2001**, *157*, 186−192.

(14) Khosrovani, N.; Korthuis, V.; Sleight, A. W.; Vogt, T. Unusual 180° P−O−P Bond Angles in ZrP_2O_7. *Inorg. Chem.* **1996**, *35*, 485−489.

(15) King, I. J.; Fayon, F.; Massiot, D.; Harris, R. K.; Evans, J. S. O. A Space Group Assignment of ZrP_2O_7 Obtained by ^{31}P Solid State NMR. *Chem. Commun.* **2001**, 1766−1767.

(16) Krogh Andersen, A. M.; Norby, P.; Hanson, J. C.; Vogt, T. Preparation and Characterization of a New 3-Dimensional Zirconium Hydrogen Phosphate τ-$Zr(HPO_4)_2$. Determination of the Complete Crystal Structure Combining Synchrotron X-ray Single-Crystal Diffraction and Neutron Powder Diffraction. *Inorg. Chem.* **1998**, *37*, 876−881.

(17) Larson, A. C.; Von Dreele, R. B. *Los Alamos National Laboratory Report LAUR 86-748;* Los Alamos National Laboratory: Los Alamos, NM, 1994.

Table 1. Crystallographic Data and Details of the Single-Crystal Data Collection

chemical formula	ZrP_2O_7
fw (g mol^{-1})	265.16
T (K)	293
wavelength (Å)	0.8000, 0.6804 (see text)
space group	*Pbca*
a (Å)[a]	24.7390(2)
b (Å)[a]	24.71841(19)
c (Å)[a]	24.7431(2)
V (Å^3)[a]	15130.6(2)
Z	108
D_c (g cm^{-3})	3.143
μ (mm^{-1})	2.511 for Mo Kα
measd reflns	532 466
unique reflns, R_{int}	27 901, 0.1122
obsd reflns ($F_o^2 > 2\sigma(F_o^2)$)	22 764
params	1222
final R1 ($F_o^2 > 2\sigma(F_o^2)$, all)	0.0493, 0.0645
final wR2, S (all)	0.1619, 1.082

[a] The unit cell parameters derived by Rietveld refinement of the high-resolution powder diffraction data have been used.

Single-Crystal Synchrotron Diffraction. A single crystal with a linear dimension of ~20 μm was used for single-crystal measurements that were performed at the station BM01A of the SNBL. Focusing optics were used in combination with a MAR345 imaging plate detector. Because of the presence of both very strong and very weak reflections, data from three independent data collections were merged together. This approach is necessary in cases such as the present because of the limited dynamic range of the detector. Two data sets were collected with a wavelength of 0.8000 Å, whereas the last was collected using $\lambda = 0.6804$ Å. The last data collection was performed 2 months after the first one, and we have no indication of any crystal decay between the two data collection periods. The first data collection was performed with a detector to crystal distance $D = 120$ mm using an oscillation angle of $\Delta\phi = 2°$ and consisted of 157 images. It covered a resolution range of $d = 7.5-0.865$ Å. The second data collection was characterized by $D = 170$ mm, $\Delta\phi = 1°$, consisted of 170 images, and covered $d = 15.0-1.131$ Å. The last data collection, performed with $\lambda = 0.6804$ Å, was performed by using $D = 90$ mm and $\Delta\phi = 2°$. It consisted of 173 images and covered $d = 5.5-0.656$ Å. The data were integrated and scaled together, thereby also correcting for variations in the incident beam intensity inherent of synchrotron radiation, using the HKL program package.[18] No absorption correction was done. The data were corrected for Lorentz and polarization effects, the latter assuming a degree of polarization of 0.95, which has been found to be appropriate for the present setup.[19] The structure was solved by using the Zr positions derived from the high-temperature phase. The P and O atoms were subsequently found by Fourier recycling techniques. This trial structure solution was performed using a partial data set consisting of data to $d_{min} = 0.865$ Å and the program JANA.[20] The final refinement using all data was done with SHELXL97.[21] Anomalous scattering factors contained in the program for Mo Kα radiation (0.710 73 Å) were used.

An additional data set was collected at 120 K to check for low-temperature phase changes (crystal-to-detector distance = 120 mm, $\Delta\phi = 2°$, $\lambda = 0.8000$ Å). These data confirmed that the sample is still orthorhombic at 120 K. A cell refinement using the CrysAlis software gave 120 K lattice parameters of $a = 24.7067(10)$, $b = 24.6829(7)$, and $c = 24.7157(9)$ Å.

Density Functional Theory Calculations. Isolated ion calculations were performed on the $P_2O_7^{4-}$ anion at the B3LYP/AUG-cc-pVDZ using Gaussian 98 with tight convergence criteria and an ultrafine DFT integration grid.[22] An initial run with loose convergence criteria starting from anion 1 from the experimental structure resulted in a C_2 symmetric anion. This symmetry was imposed in the final calculation. Vibrational analysis confirmed that the structure obtained is a minimum on the potential energy surface. The calculated structural parameters are given in Table 5. In a second run, again with tight convergence criteria and an ultrafine DFT integration grid, a relaxed potential energy surface scan was made of the P−O$^{\mu}$−P angle from 105 to 179.9°.

Results

The ZrP_2O_7 samples used for the present study were prepared at a fairly low temperature, 240 °C, which is several hundred degrees below the temperature used by Korthuis et al.[12] Most importantly, the synthesis temperature is below the phase transition temperature leading to the supercell, which was determined to be at 290 °C by Korthuis et al.[12] using differential scanning calorimetry (DSC), so that it should be possible to obtain nontwinned crystals. As seen below, this is indeed the case. In contrast to crystals most often obtained by solid-state methods, the crystals obtained by our synthesis method are very well dispersed with well developed facets. The single crystals obtained had linear dimensions up to ~20 μm (see Figure 1) and their shape is close to octahedral, reflecting that the symmetry is close to cubic.

To look for possible lattice distortions, we used high-resolution synchrotron powder diffraction at the SNBL at the ESRF in Grenoble, France. This installation provides one of the highest instrumental resolutions in the world. The powder diffractogram showed clear, though very small, deviations from cubic metric symmetry. Figure 2 shows one of the parent-phase peaks, (0 6 12) (cubic indexing), which would not be split if the symmetry was cubic. The refined room-temperature lattice, Table 1, shows that the deviation from the average lattice parameter (24.7335(2) Å) is 0.0055(3), −0.0151(3), and 0.0096(3) Å for a, b, and c, respectively. These very small differences amount to 0.022%, 0.061%, and 0.039% of the average. The largest difference between

(18) Otwinowski, Z.; Minor, W. Processing of X-ray Diffraction Data Collected in Oscillation Mode. In *Macromolecular Crystallography, A;* Carter, C. W., Jr., Sweet, R. M., Eds.; Methods in Enzymology, Vol. 276; Academic Press: New York, 1997; pp 307−326.
(19) Birkedal, H. Uses of Synchrotron Radiation in Chemical Crystallography. Ph.D. Thesis, University of Lausanne, Lausanne, Switzerland, 2000.
(20) Petricek, V.; Dusek, M. *Jana2000. The Crystallographic Computing System;* Institute of Physics: Praha, Czech Republic, 2000.
(21) Sheldrick, G. M. *SHELXL-97: Program for the Refinement of Crystal Structures;* University of Göttingen: Göttingen, Germany, 1997.
(22) Frisch, M. J.; Trucks, G. W.; Schlegel, H. B.; Scuseria, G. E.; Robb, M. A.; Cheeseman, J. R.; Zakrzewski, V. G.; Montgomery, J. A., Jr.; Stratmann, R. E.; Burant, J. C.; Dapprich, S.; Millam, J. M.; Daniels, A. D.; Kudin, K. N.; Strain, M. C.; Farkas, O.; Tomasi, J.; Barone, V.; Cossi, M.; Cammi, R.; Mennucci, B.; Pomelli, C.; Adamo, C.; Clifford, S.; Ochterski, J.; Petersson, G. A.; Ayala, P. Y.; Cui, Q.; Morokuma, K.; Malick, D. K.; Rabuck, A. D.; Raghavachari, K.; Foresman, J. B.; Cioslowski, J.; Ortiz, J. V.; Stefanov, B. B.; Liu, G.; Liashenko, A.; Piskorz, P.; Komaromi, I.; Gomperts, R.; Martin, R. L.; Fox, D. J.; Keith, T.; Al-Laham, M. A.; Peng, C. Y.; Nanayakkara, A.; Gonzalez, C.; Challacombe, M.; Gill, P. M. W.; Johnson, B. G.; Chen, W.; Wong, M. W.; Andres, J. L.; Head-Gordon, M.; Replogle, E. S.; Pople, J. A. *Gaussian 98*, revision A.7; Gaussian, Inc.: Pittsburgh, PA, 1998.

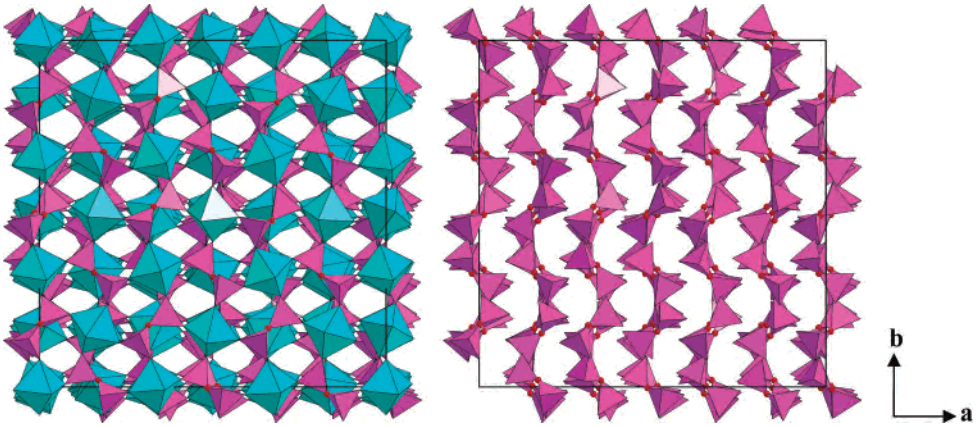

Figure 3. Crystal structure of ZrP_2O_7 shown in projection along the *c*-axis. Cyan octahedra and purple tetrahedra mark the ZrO_6 and PO_4 units, respectively. The bridging oxygen atom in the $P_2O_7^{4-}$ anions is shown as a red sphere. The figure on the right shows only the $P_2O_7^{4-}$ part of the structure.

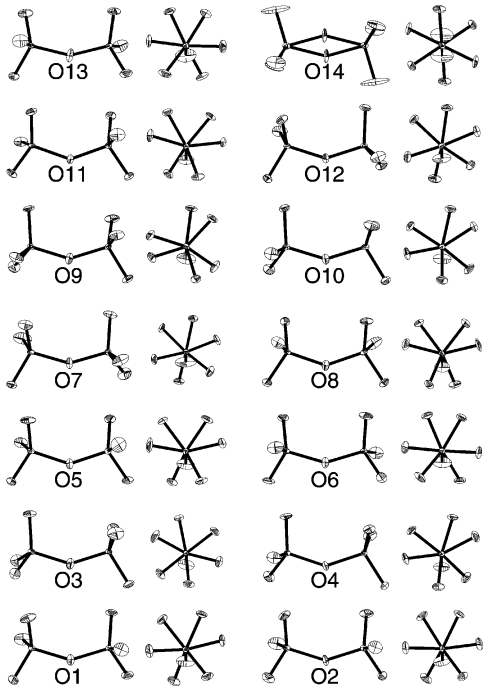

Figure 4. Comparison of the $P_2O_7^{4-}$ ions. For each ion, two projections are shown: onto the P−O$^{\mu}$−P plane and perpendicular thereto (along the P−P axis). Note the very large variation in O^{t}−P−O$^{\mu}$−P torsion angles. The atoms are shown as 50% probability density ellipsoids. Ion 14 is disordered and situated on a symmetry element; thus, only half the ion is unique.

lattice parameters is between *c* and *b*, 0.0247(3) Å, which is 0.100(1)% of the average. The small size of the orthorhombic distortion underlines the power and necessity of high-resolution synchrotron powder diffraction. The distortion was not detectable in the neutron powder diffraction data available to Khosrovani et al.[14]

The orthorhombic structure was successfully determined from single-crystal synchrotron diffraction data. The structure consists of ZrO_6 octahedra, which are corner linked to PO_4 tetrahedra. Two tetrahedra are connected through the bridging oxygen, O$^{\mu}$, to form the $P_2O_7^{4-}$ anion. The structure is shown in Figure 3. A key conclusion of the present work is that the structure is indeed orthorhombic and that none of the pyrophosphate anions have 180° P−O−P bond angles. There are 14 pyrophosphate ions in the asymmetric unit, one of

Table 2. Overview of Coordination Geometry[a]

entity	*N*	min	max	average	σ^b
Zr−O	84	2.032(3)	2.088(3)	2.058	0.012
	81	2.032(3)	2.088(3)	2.058	0.012
P−O^{t}	81	1.481(3)	1.515(3)	1.504	0.007
	78	1.490(3)	1.515(3)	1.504	0.006
P−O$^{\mu}$	28	1.540(7)	1.602(7)	1.574	0.011
	26	1.560(3)	1.584(3)	1.574	0.007
P−O$^{\mu}$−P	14	140.7(2)	152.4(3)	145.6	3.1
	13	140.7(2)	152.4(3)	145.3	2.9
O^{t}−P−O$^{\mu}$ (small)	42	100.1(4)	120.6(3)	105.7	3.7
	39	102.81	109.2	105.2	1.8
O^{t}−P−O$^{\mu}$ (large)	42	90.9(3)	112.0(4)	107.5	3.4
	39	104.11(17)	110.37(16)	108.1	1.6
O^{t}−P−O^{t}	81	110.34(16)	113.66(17)	112.1	0.8
	78	110.34(16)	113.66(17)	112.1	0.8
O−Zr−O_{180}	42	172.39(12)	180.00	176.5	2.0
O−Zr−O_{90}	168	83.95(11)	97.75(12)	90.0	2.2

[a] *N* is the number of bond distances/angles of a given type while the range of observed values is expressed by min and max. The average and the standard deviation from the mean, $\sigma = (\sum_i(d_i - \langle d_i\rangle)^2)^{1/2}/(N-1)$, are also reported. For each entity, two lines are given: with (first line) and without (second line) the disordered pyrophosphate 14. [b] $\sigma = (\sum_i(d_i - \langle d_i\rangle)^2)^{1/2}/(N-1)$.

which (P14, O14, O14A, O14B, and O14C, with O14 being the bridging oxygen) is situated on a symmetry element in agreement with the space group assignment derived by solid-state NMR.[15] Even for the P14 pyrophosphate ion, the data clearly showed that the bridging oxygen is not 180° on average but a distinct asymmetric, albeit disordered, position was found for the bridging oxygen atom.

An overview of the average geometrical parameters is given in Table 2. The disordered pyrophosphate ion, number 14, is an outlier in the distribution of most of the geometrical descriptors, and Table 2 presents averages both with and without ion 14. The spread of both distances and angles is somewhat larger than the standard uncertainty of each observation. The individual pyrophosphate ions are shown in Figure 4, which displays the atomic displacement parameter ellipsoids while Figure 5 displays distributions of the O−P−O angles. All the pyrophosphates display large amplitudes for the motion of O$^{\mu}$ perpendicular to the P−O$^{\mu}$−P plane. As is evident from Figure 4 and from the O^{t}−P−O$^{\mu}$−P reported in Table 4, there is a very large variation in the orientation of the PO^{t}_3 group with respect to the P−O$^{\mu}$−P plane. Thus, there appears to be essentially no

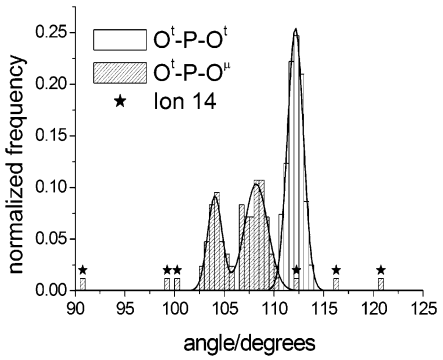

Figure 5. Histograms showing the distributions of O^t-P-O^t (open boxes) and O^t-P-O^μ (hatched boxes) angles. The angles involving O14 are indicated with a star. The full lines represent Gaussian fits to the two distributions.

Table 3. Coordination Geometry of the Individual Zr Atoms

	⟨Zr−O⟩ (Å)	$rmsd_{Zr-O}$ (Å)	angular rmsd (deg)
Zr1	2.060	0.014	1.18
Zr2	2.052	0.009	1.38
Zr3	2.056	0.007	4.04
Zr4	2.059	0.013	4.24
Zr5	2.055	0.015	2.47
Zr6	2.062	0.008	3.10
Zr7	2.065	0.013	1.94
Zr8	2.060	0.018	2.57
Zr9	2.061	0.008	2.29
Zr10	2.055	0.011	2.47
Zr11	2.059	0.010	1.67
Zr12	2.057	0.012	1.82
Zr13	2.053	0.010	1.53
Zr14	2.055	0.012	3.73

constraint on the orientation of the terminal group around the $P-O^\mu-P$ plane. The two PO^t_3 groups in each pyrophosphate are almost staggered.

The DFT calculations on the isolated ion showed it to have an equilibrium $P-O^\mu-P$ angle of 153.4°, a little larger than the average in the experimental structure, 145.6(3.1)°. The optimized structure is shown in Figure 6a and described in Table 5, which also lists the three lowest normal modes. Mulliken charge analysis indicates that the negative charges are evenly distributed over the oxygen atoms: the charges are −1.080 for O^μ, 1.749 for each of the P-atoms, and −1.076, −1.069, and −1.064 for O^{t1}, O^{t2}, and O^{t3}, respectively. The relaxed potential energy surface (PES) of the $P-O^\mu-P$ angle is shown in Figure 6b. The resulting potential

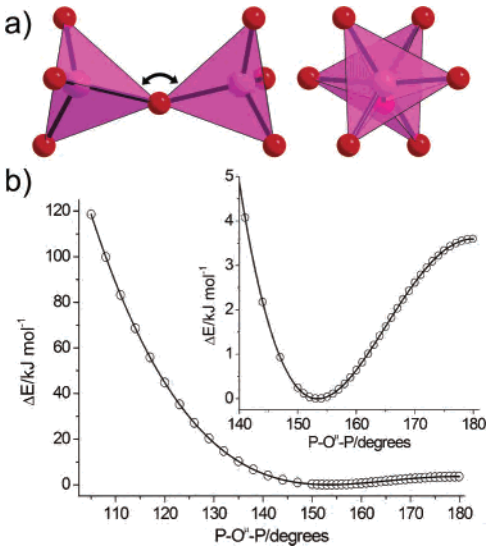

Figure 6. Results of DTF calculations on the isolated $P_2O_7^{4-}$ ion at the B3LYP/AUG-cc-pVDZ level: (a) optimized structure with views onto the $P-O^\mu-P$ plane (left) and perpendicular thereto (right); (b) relaxed $P-O^\mu-P$ potential energy surface scan, indicated by the arrow in part a. The solid line represents a fit to a 12th order polynomial with all odd order coefficients equal to zero.

energy surface could be modeled by a 12th order polynomial with all odd coefficients equal to zero: $\Delta E(\alpha) = \sum_{i=0,2,...,12} a_i (\alpha - \alpha_0)^i$ where α is the $P-O^\mu-P$ angle. The coefficients derived by least-squares are $\alpha_0 = 180°$, $a_0 = 3.5928$ kJ mol^{-1}, $a_2 = -0.01061$ kJ mol^{-1} deg^{-2}, $a_4 = 8.5024 \times 10^{-6}$ kJ mol^{-1} deg^{-4}, $a_6 = -1.093 \times 10^{-9}$ kJ mol^{-1} deg^{-6}, $a_8 = 1.723 \times 10^{-13}$ kJ mol^{-1} deg^{-8}, $a_{10} = -1.752 \times 10^{-17}$ kJ mol^{-1} deg^{-10}, $a_{12} = 8.324 \times 10^{-22}$ kJ mol^{-1} deg^{-12}. At angles lower than the equilibrium, the energy increases very rapidly. However, for larger angles the PES is fairly shallow, and the inversion barrier at 180° is only 3.60 kJ mol^{-1}. For comparison, this is 6.5 times smaller than the inversion barrier in ammonia.[23] The equilibrium structure has two low-frequency modes with $\nu < 31$ cm^{-1} (Table 5). As could be expected, the lowest frequency mode corresponds to a movement of the bridging oxygen atom out of the $P-O^\mu-P$ plane and an accompanying deformation of the terminal oxygen umbrella-like shape. It is evident from the large transverse amplitude of the O^μ atomic displacement parameters (Figure 4) that a similar mode is active in the crystal.

Table 4. Torsion Angles (deg) of the $P_2O_7^{4-}$ Ions

ion	O*i*A−P*i*A−O*i*−P*i*B	O*i*B−P*i*A−O*i*−P*i*B	O*i*C−P*i*A−O*i*−P*i*B	O*i*D−P*i*B−O*i*−P*i*A	O*i*E−P*i*B−O*i*−P*i*A	O*i*F−P*i*B−O*i*−P*i*A
1	80.6(5)	−161.5(5)	−40.6(5)	−145.2(5)	97.3(5)	−25.3(5)
2	87.6(4)	−154.3(4)	−33.6(5)	−147.4(4)	93.9(4)	−27.3(5)
3	110.0(4)	−133.5(4)	−12.0(5)	−175.7(4)	65.4(5)	−55.5(5)
4	138.8(3)	−103.3(4)	18.0(4)	175.1(3)	55.0(4)	−66.3(4)
5	82.4(4)	−158.7(4)	−38.8(4)	−155.1(4)	85.7(4)	−35.8(4)
6	151.8(5)	−89.3(5)	32.0(5)	144.1(5)	24.2(5)	−97.9(5)
7	72.6(6)	−168.0(6)	−47.7(7)	−133.2(6)	107.6(6)	−12.7(7)
8	160.0(3)	−80.7(4)	39.9(4)	159.8(3)	39.0(4)	−81.8(4)
9	129.9(4)	−112.9(5)	8.0(5)	−165.2(4)	76.6(5)	−45.4(5)
10	133.7(4)	−106.8(5)	13.3(5)	−61.2(5)	60.5(5)	180.0(4)
11	90.1(4)	−151.5(3)	−30.6(4)	−161.7(3)	78.7(4)	−42.1(4)
12	71.5(4)	−169.3(4)	−49.8(5)	−129.4(4)	113.3(4)	−8.4(5)
13	154.0(6)	−86.8(7)	33.6(7)	−94.8(7)	26.5(7)	145.9(6)
14	126.7(14)[a]	4.8(17)[a]	−118.9(14)[a]			

[a] O14*k*−P14−O14−P14$^{(i)}$, i = 1 − *x*, 1 − *y*, 1 − *z*.

Table 5. Structural Parameters of an Isolated $P_2O_7^{4-}$ Ion Calculated at the B3LYP/AUG-cc-pVDZ Level[a]

Cartesian Coordinates			
atom	*x*	*y*	*z*
O^{μ}	0	0	0.395 475
P	0	1.681 750	−0.001 737
O^{t1}	−0.716 069	2.348 456	1.260 265
O^{t2}	1.521 717	2.133 924	−0.110 997
O^{t3}	−0.806 050	1.928 043	−1.343 748

Three Lowest Normal Modes									
	ν_1/B (mode/symmetry) 18.79 ν/cm^{-1}			ν_2/A (mode/symmetry) 30.72 ν/cm^{-1}			ν_3/A (mode/symmetry) 96.07 ν/cm^{-1}		
atom	q_x	q_y	q_z	q_x	q_y	q_z	q_x	q_y	q_z
O^{μ}	0.65	0.00	0.00	0.00	0.00	−0.02	0.00	0.00	−0.52
P	0.00	0.00	0.00	0.02	0.00	0.00	0.00	0.10	−0.01
O^{t1}	−0.16	−0.18	0.00	−0.33	−0.03	−0.18	0.00	−0.25	0.16
O^{t2}	−0.11	0.41	0.01	0.04	0.05	0.41	−0.01	0.12	0.07
O^{t3}	−0.05	−0.23	0.00	0.37	−0.01	−0.21	−0.01	0.49	0.05

[a] C_2 symmetry was imposed. Only the unique atoms are given; the remaining atoms are generated by the symmetry operation ($-x$, $-y$, z). For the normal modes, the deformation vectors for the remaining atoms are generated by the symmetry operations (q_x, q_y, $-q_z$) and ($-q_x$, $-q_y$, q_z) for B and A symmetry modes, respectively. The total energy is −1209.002 181 hartree while the zero point energy is 63.31 hartree.

The second lowest mode is essentially a pure PO_3 deformation mode, with the P atoms and the bridging oxygen almost stationary. Only the third mode, $\nu = 96.1$ cm^{-1}, is a P−O^{μ}−P bending mode. This shows that in the isolated anion, the vibration tending toward a linear bond is not the lowest frequency one.

The Zr atoms are octahedrally coordinated with an average Zr−O distance of 2.058(12) Å as shown in Table 2. Table 3 gives a summary of the coordination geometry around the individual Zr atoms. The octahedra are distorted but only to a small extent; the root mean square deviation (rmsd) from 90° is in the range 1.18−4.24°. Interestingly, there is a tendency for a negative correlation between the P−O distance and the P−O−Zr angle; that is, the P−O distance is smaller for larger values of the P−O−Zr angles, and the correlation coefficient R is −0.6393.

Discussion and Conclusion

The present work is based on some key technical advances compared to previous work. Our low-temperature synthesis route was a key facilitator for the single-crystal diffraction study since it provided access to single, untwinned crystals. The high-resolution synchrotron powder diffraction data clearly showed, Figure 2, that the lattice is not metrically cubic and allowed precise determination of the orthorhombic lattice parameters. The availability of single crystals allowed structure determination by single-crystal techniques. Because of the very weak superstructure reflections and large unit cell, the single-crystal study necessitated the use of area detectors and synchrotron radiation. It should be stressed that these techniques are becoming more and more readily available as the numbers of synchrotron facilities continues to grow.

The barrier to inversion of the free pyrophosphate ion was by DFT found to be 3.60 kJ mol^{-1}, which is equivalent to 433 K if converted using the k_BT relationship with k_B being the Boltzmann constant. Thus, if the only factor influencing the phase transition temperature would be the barrier to inversion of the pyrophosphate ion, one would expect the phase transition to the P−O−P disordered cubic phase to occur at this temperature. The experimentally observed transition temperature is somewhat higher, 563 K. However, the isolated ion calculations are approximate and, most importantly, do not take Zr-coordination and interion interactions into account. If we transform the observed transition temperature to an effective barrier, a value of 4.7 kJ mol^{-1} is obtained for the "effective inversion barrier".

Acknowledgment. We thank the staff of the Swiss−Norwegian Beam Line for their kind assistance, Professor Dieter Schwarzenbach for helpful discussions, and the Swiss National Science Foundation for financial support (Grant No. 20-105325). We thank Mr. G. Burri and the late Mr. G. Troillet for the microprobe measurements and the SEM pictures. H.B. is a Steno research assistant professor funded by the Danish Natural Sciences Research Council and the Danish Technical Research Council. He thanks the Danish Research Training Council and the Danish Natural Sciences Research Council for additional financial support. The Swiss−Norwegian Beam Lines is funded by the Norwegian Research Council and the Swiss State Secretariate for Education and Research (SER).

Supporting Information Available: Crystallographic data in CIF format; illustration of anion modes. This material is available free of charge via the Internet at http://pubs.acs.org.

IC0600174

(23) Cotton, F. A.; Wilkinson, G. *Advanced Inorganic Chemistry;* John Wiley & Sons: New York, 1988; p 307.